Reactions of Unsymmetric Chiral Dialdehydes with Lysine: Regio- and Enantioselective Macrocyclization and Fluorescent Sensing

Yifan Mao, Yichen Li, Stephanie Davis, and Lin Pu*

Department of Chemistry, University of Virginia, Charlottesville, Virginia 22904, USA.
E-mail: lp6n@virginia.edu

Received Date (will be automatically inserted after the manuscript is accepted)

Abstract. Three BINOL-based unsymmetric chiral dialdehydes, (*S*)-**4**, (*S*)-**5**, and (*S*)-**6**, each containing a salicylaldehyde moiety and an *ortho*-, *meta*- or *para*-substituted benzaldehyde unit, are synthesized and used to react with the enantiomers of an unsymmetric chiral diamine, lysine. These reactions represent the first examples of regioselective as well as enantioselective reactions of an unsymmetric chiral dialdehyde with an unsymmetric chiral diamine to generate unsymmetric chiral macrocycles. The addition of Zn^{2+} can further enhance the selectivity for the macrocycle formation. Compounds (*S*)-**4** and (*S*)-**5** are found to exhibit chemoselective and enantioselective fluorescent recognition of lysine in the presence of Zn^{2+}.

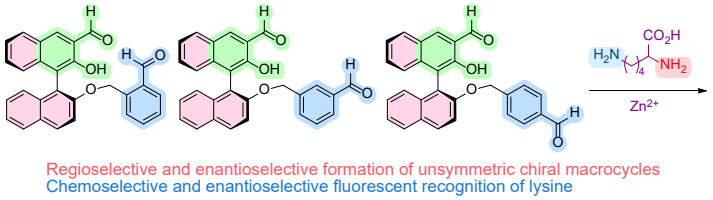

1. INTRODUCTION

1,1'-Bi-2-naphthol (BINOL)-based C_2 symmetric chiral aldehydes such as (*S*)-**1**,[1] (*R*)-**2**,[2] and (*S*)-**3**[3] (Figure 1) have been used to react with symmetric chiral and achiral diamines or tetraamines to make chiral materials such as macrocycles and covalent organic networks for applications in asymmetric catalysis, molecular recognition and fluorescent sensing. These syntheses utilize the reversible imine formation from the condensation of aldehydes with amines to generate the thermodynamically most stable structures. In the construction of the structurally well-defined materials via the dynamic covalent chemistry of imines,[4,5] the symmetries of both the aldehydes and amines are important in order to avoid the formation of regioisomeric mixtures in the resulting cages, macrocycles, metal organic networks and covalent organic networks.[1-3,6,7] No reaction of unsymmetric chiral aldehydes with unsymmetric chiral amines was used to conduct a regioselective and enantioselective synthesis of unsymmetric chiral macrocycles until our recent communication on this subject.[8]

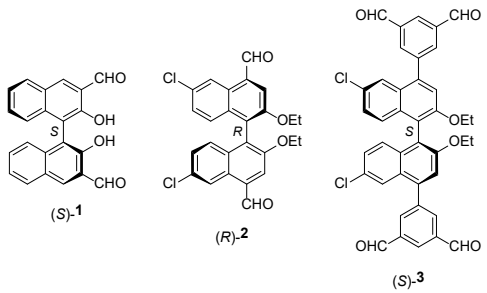

Figure 1. Examples of BINOL-based C_2 symmetric chiral aldehydes.[1~3]

We have designed a series of BINOL-based unsymmetric chiral dialdehydes including (*S*)-**4,** (*S*)-**5**, and (*S*)-**6** for materials synthesis (Figure 2). These BINOL-based compounds contain an *ortho*-, *meta*- or *para*-substituted benzaldehyde unit and a salicylaldehyde moiety that has an adjacent hydroxy group. The salicylaldehyde unit is expected to undergo a faster reaction with a primary amine to form a more stable imine product due to an intramolecular hydrogen bond with the adjacent hydroxy group than the benzaldehyde unit does.[9] Lysine (Lys) is an unsymmetric chiral diamine containing a more basic ε-amine group that should be more reactive with an aldehyde than the less basic α-amine group. Our study on the reactions of (*S*)-**4,** (*S*)-**5**, and (*S*)-**6** with the enantiomers of Lys has led to the discovery of a highly regioselective as well as enantioselective process for the formation of unsymmetric chiral macrocycles. It is also found that the presence of Zn^{2+} can further enhance the selectivity of the reactions. These selective reactions have led to chemoselective as well as enantioselective fluorescent recognition of Lys. Herein, these results are reported.[8]

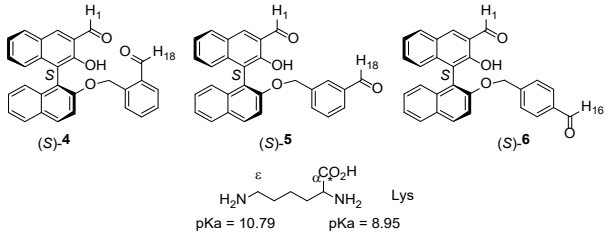

Figure 2. BINOL-based unsymmetric chiral dialdehydes.

2. RESULTS AND DISCUSSION

a. Synthesis of (*S*)-4, (*S*)-5, and (*S*)-6.

The unsymmetric chiral dialdehydes (*S*)-**4**, (*S*)-**5**, and (*S*)-**6** are readily synthesized from the reaction of the BINOL-based monoaldehyde (*S*)-**7**[10] with *ortho*-, *meta*- or *para*-bromomethyl-benzaldehyde in the presence of K_2CO_3 followed by the removal of the MOM group under acidic conditions (Scheme 1). The ^{1}H

Scheme 1. Synthesis of Compounds (*S*)-**4**, (*S*)-**5**, and (*S*)-**6**.

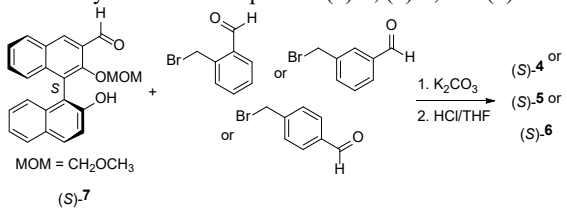

NMR spectrum of (*S*)-**4** in DMSO-d_6 gives two aldehyde signals at δ 10.32 (proton 1) and 9.99 (proton 18). The intramolecular hydrogen bonding with the *ortho*-hydroxy group has shifted the

proton 1 signal of the salicylaldehyde unit of (*S*)-**4** more down-field than that of the benzaldehyde unit. This hydrogen bonding also leads to a highly down-field-shifted hydroxy signal at δ 10.18. Similarly, (*S*)-**5** in DMSO-d_6 gives two aldehyde signals at δ 10.34 (proton 1), 9.76 (proton 18), and the hydroxy signal at δ 10.23; (*S*)-**6** in DMSO-d_6 gives two aldehyde signals at δ 10.34 (proton 1), 9.90 (proton 16), and the hydroxy signal at δ 10.23. See Figures S1 to S14 in SI for 1D and 2D NMR spectra of these compounds with more detailed signal assignments.

b. Study of the Reaction of (*S*)-4 with the Sodium Salt of Lys.

We studied the interaction of (*S*)-**4** with the sodium salt of L-Lys (L-Lys$^-$), prepared by treating L-Lys with a 1:1 ratio of sodium hydroxide in methanol followed by evaporation of the solvent. ^{1}H NMR spectroscopy was utilized to monitor the reaction of (*S*)-**4** with 0 ~ 2 equiv of L-Lys$^-$ in DMSO-d_6 at room temperature over 10 h (Figure 3, see Figure S15 in SI for the reactions with up to 4.0 equiv L-Lys$^-$). The ^{1}H NMR data in Figure 3 indicate that in the presence of 2 equiv L-Lys$^-$, there was a predominant formation of a single product. Comprehensive analysis using both 1D and 2D NMR techniques, including ^{1}H, ^{13}C, HSQC, and TOCSY spectra (with detailed signal assignments available in Figures S16 to S19 in SI), led to the establishment of a macrocyclic structure for the observed product, designated as compound **8** (Figure 4). The structure of compound **8** was characterized by distinctive imine proton signals at δ 8.58 (proton 1) and δ 8.44 (proton 18). TOCSY/NOESY correlations were identified between the imine proton 1 and the α-proton 23 (δ 3.57), as well as between the imine proton 18 and the ε-protons 19 (δ 3.55 and 3.41), as detailed in Figures S17 and S18 in SI. The observed correlation between the α-proton 23 and the ε-protons 19 in the TOCSY spectrum further confirmed the macrocyclic configuration. Additionally, the TOF mass spectrometry (ES+) revealed a predominate signal at m/z = 543.2292 for compound **8** (calculated for **8**+2H: 543.2284) (see Figure S20 in SI).

Figure 3 shows that when (*S*)-**4** was treated with 1.0 equiv L-Lys$^-$, a mixture of two compounds was generated. The major product was identified as a regioisomer of **8**, referred to as compound **9** (Figure 4, established by HSQC, NOESY, and TOCSY, see Figures S21 to S24 in SI), while the minor product is **8**. For compound **9**, the imine protons are observed at δ 8.72 (proton 1) and δ 8.30 (proton 18). Similar to **8**, the macrocyclic structure of compound **9** is confirmed through the correlation of these imine protons with ε-protons 23 and α-proton 19, as revealed in the TOCSY spectrum. A distinctive peak at δ 13.90 is attributed to the hydroxy proton in **9**. This hydroxy signal is notably shifted downfield compared to that of (*S*)-**4**, indicating the formation of a stronger intramolecular hydrogen bond in this imine product than that in the aldehyde precursor. In the presence of an excess amount of L-Lys$^-$ (2.0 equiv), compound **9** was mostly converted to compound **8**. Additionally, this excess L-Lys$^-$ should facilitate a rapid exchange of the hydroxy proton, resulting in the disappearance of the hydroxy signal at δ 13.90.

In the TOF mass spectrum of the mixture resulting from the reaction of (*S*)-**4** with 1.0 equiv of L-Lys$^-$, a peak at m/z = 543.2281 can be attributed to both compounds **9** and **8** (calculated for **9**+2H or **8**+2H: 543.2284) (see Figure S25 in SI). Additionally, two peaks at m/z = 561.2396 and 531.2284 are identified, corresponding to the monoaldehyde **10**+2H (calculated: 561.2389) and **10**+2H−HCO (calculated: 531.2284), respectively. The presence of the monoaldehyde **10** (Figure 4) is further corroborated by the ^{1}H NMR spectrum of the reaction between (*S*)-**4** and 1.0 equiv of L-Lys$^-$, as illustrated in Figure 3. This spectrum reveals the absence of the salicylaldehyde signal from (*S*)-**4** at δ 10.32, while a very small benzaldehyde signal is observed at δ 9.98, indicating a faster reaction of the salicylaldehyde group than the benzaldehyde group in forming the intermediate **10**. This monoaldehyde could also be generated from the partial hydrolysis of **8** and **9** under the mass analysis conditions, as also observed in the mass spectrum for the reaction of (*S*)-**4** with 2.0 equiv L-Lys$^-$, where no aldehyde signal was present.

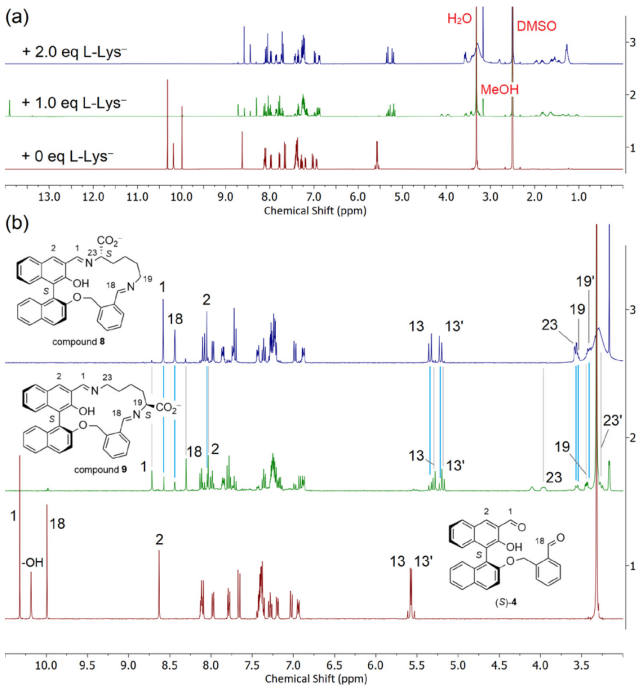

Figure 3. (a) ^{1}H NMR (800 MHz) spectra of (*S*)-**4** (4.0 mM) + 0 ~ 2.0 equiv L-Lys$^-$ in DMSO-d_6. (Reaction time: rt for 10 h). (b) zoomed regions with signal assignments.

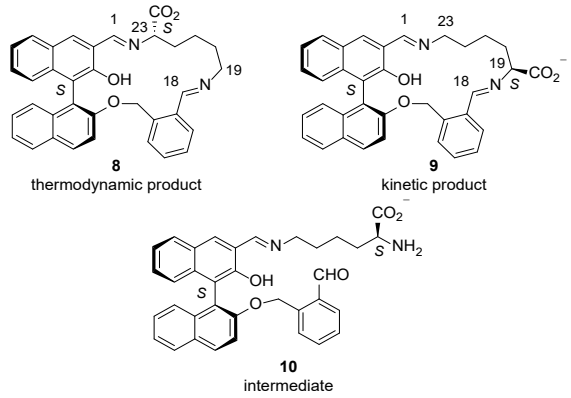

Figure 4. Structures of compounds **8**, **9**, and **10**.

The progression of the reaction between (*S*)-**4** and 2.0 equiv of L-Lys$^-$ was tracked from 10 min to 10 h through ^{1}H NMR spectroscopy, as shown in Figures S26 and S27 in SI. In 10 min, (*S*)-**4** was found to undergo a complete conversion to compounds **9** (major) and **8** (minor). In 10 h, the reaction reached an equilibrium to give compound **8** at 92.8% and compound **9** at 7.2%. This indicates that **9** should be a kinetic product due to its rapid formation which was then converted to a thermodynamically more stable product **8**. Thus, the reaction of (*S*)-**4** with L-Lys$^-$ leads to the formation of the unsymmetric chiral macrocycle **8** with high regioselectivity.

On the basis of the above investigation, a mechanism for the reaction of (*S*)-**4** with L-Lys$^-$ is proposed in Scheme 2. Initially, when (*S*)-**4** is treated with L-Lys$^-$, the reaction between the more reactive salicylaldehyde moiety of (*S*)-**4** and the more nucleophilic ε-NH_2 group of L-Lys$^-$ is anticipated to be the fastest step among the four competing amine-aldehyde condensation reactions, leading to the formation of the intermediate **10**. This step is

followed by an intramolecular condensation to convert **10** to the kinetic product **9**. Subsequently, the thermodynamic product **8** emerges from the intramolecular condensation of intermediate **11**, generated via the condensation of the salicylaldehyde unit of (*S*)-**4** with the less nucleophilic α-NH_2 group of L-Lys$^-$. In the case of both intermediates **10** and **11**, the benzaldehyde component, being less reactive, shows a preference to undergo intramolecular reactions, thereby favoring the formation of macrocycles rather than engaging in the less advantageous intermolecular reactions that would lead to the formation of higher oligomers and polymers. Compound **9** can also react with excess L-Lys$^-$ to form an acyclic diimine intermediate **12** which can then undergo an intramolecular reaction to give **8**. Consequently, the disparate reactivity profiles of the two aldehyde groups present in (*S*)-**4**, along with those of the two amino groups of L-Lys$^-$, in conjunction with the stability variance between the resulting products, culminate in a highly regioselective macrocyclization that forms **8**.

Scheme 2. Proposed Reaction Mechanism for (*S*)-**4** with L-Lys$^-$.

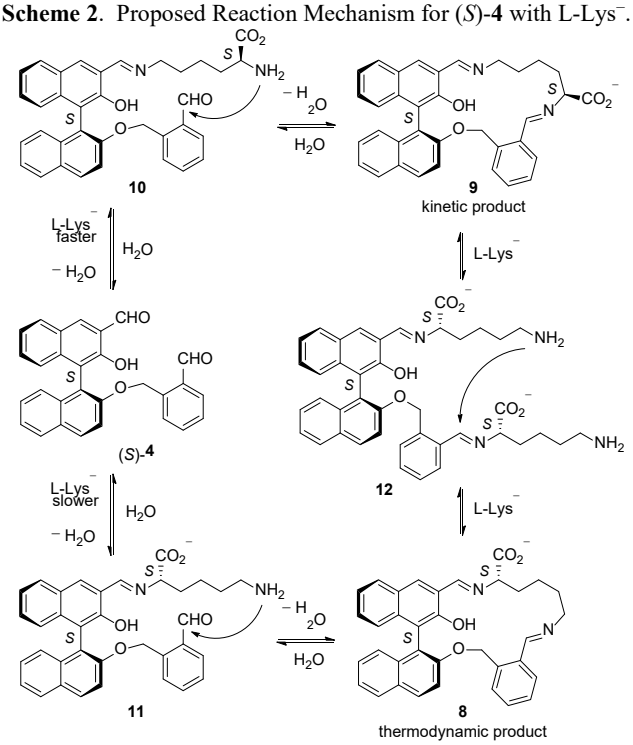

We also studied the reaction of (*S*)-**4** with 0 ~ 4 equiv D-Lys$^-$, the enantiomer of L-Lys$^-$, in DMSO-d_6 and the resulting NMR spectra are compiled in Figure S28 in SI. Upon reacting (*S*)-**4** with 1.0 equiv of D-Lys$^-$ at room temperature for 10 h, a predominant product, identified as compound **13** (Figure 5), was formed. The structure of compound **13** was established through 1D and 2D NMR spectroscopic analyses, with detailed signal assignments and mass spectrometry data presented in Figures S29 to S33 in the Supplementary Information. Introducing 2.0 equiv of D-Lys$^-$ resulted in the complete conversion of (*S*)-**4** to a mixture of **13** and **14** (Figure 5). (see Figures S34 ~ S38 in SI for detailed 1D and 2D NMR signal assignment and mass spectrum)

The reaction of (*S*)-**4** with 2.0 equiv of D-Lys$^-$ was also monitored from 10 min to 10 h by ^{1}H NMR spectroscopy as shown in Figures S39 and S40. It was found that in 10 min, (*S*)-**4** was completely converted to compounds **13** (major) and **14** (minor). The reaction attained equilibrium after 10 h, resulting in a product distribution of 32.6% for compound **13** and 67.4% for compound **14**. The formation of compound **13** as the kinetic product is attributed to the initial reaction of the more reactive salicylaldehyde unit of (*S*)-**4** with the more nucleophilic ε-NH_2 group of D-Lys$^-$, leading to an intermediate analogous to compound **10** (as proposed in Scheme 2), which subsequently undergoes intramolecular condensation. Following a mechanism similar to that depicted in Scheme 2, the reaction leads to the formation of the slightly more stable compound **14** as the major product.

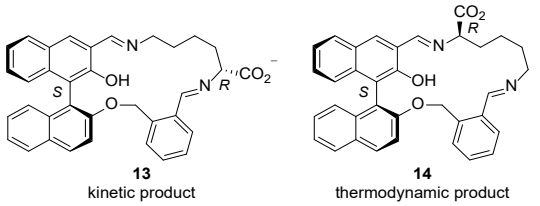

Figure 5. Structures of compounds **13** and **14**.

The reactivity of (*S*)-**4** with L-Lys$^-$ versus that with D-Lys$^-$ was further investigated by examining the reaction of (*S*)-**4** with 2 equiv of the racemic Lys salt (*rac*-Lys$^-$). The observations, as shown in Figures S41 and S42 in SI, reveal that within 10 min, (*S*)-**4** underwent complete conversion into a mixture of four macrocyclic compounds: **8**, **9**, **13,** and **14**. Notably, the kinetic products **9** and **13** were formed predominantly in comparable amounts, with yields of 52% for **9** and 31% for **13**. This similarity in formation rates between the intermediate **10** derived from L-Lys$^-$ and its diastereomeric counterpart from D-Lys$^-$ suggests similar reactivities, attributed to the distance between the chiral center of the Lys unit and the chiral BINOL unit. The subsequent facile intramolecular condensation reactions of **10** and its diastereomer lead to the formation of their respective macrocycles **9** and **13**. Upon reaching equilibrium after 20 h, the reaction mixture exhibited enantioselective formation of the thermodynamic product **8** in a 68% yield. This outcome underscores the selective influence of the chirality of L-Lys$^-$ in steering the reaction towards the preferential formation of compound **8**, illustrating the intricate dynamics of stereochemistry in the synthesis of macrocyclic compounds. These findings demonstrate that the reaction of (*S*)-**4** with Lys$^-$ exhibits both regioselectivity and enantioselectivity in the production of the unsymmetric chiral macrocycle **8**.

In light of the previous findings that the C_2 symmetric chiral dialdehyde (*S*)-**1** undergoes stereoselective reactions with amino acids in the presence of Zn^{2+},[10,11] we sought to investigate the influence of Zn^{2+} on the reactivity of the unsymmetric chiral dialdehyde (*S*)-**4** with Lys$^-$. As shown in Figure 6 (see Figure S43 for the full spectra), the macrocycle **8**, formed from the reaction of (*S*)-**4** with 2.0 equiv L-Lys$^-$ over 10 h, produced a single Zn-complex upon addition of 2.0 or more equiv of Zn^{2+}. Through 1D and 2D NMR spectroscopy, including ^{1}H, HSQC, and TOCSY, the presence of two distinct imine signals at δ 8.63 and 8.19 was observed upon the introduction of 4.0 equiv of Zn^{2+} (see Figures S44 to S51). These imine signals exhibited TOCSY correlations with adjacent protons 23 and 19, indicating that the macrocyclic structure of compound **8** is preserved in the resulting Zn^{2+} complex. The addition of excess Zn^{2+} might have saturated the coordination sites available on the heteroatoms of the macrocycle, leading to the well-defined NMR signals for the end product whose structure has not been fully established yet. In the mass spectroscopic analysis of macrocycle **8** in the presence of an excess amount of Zn^{2+}, the Zn-complex was not detected, likely due to the instability of the Zn coordination under the mass spectroscopic conditions (see Figures S52 and S53 for more details).

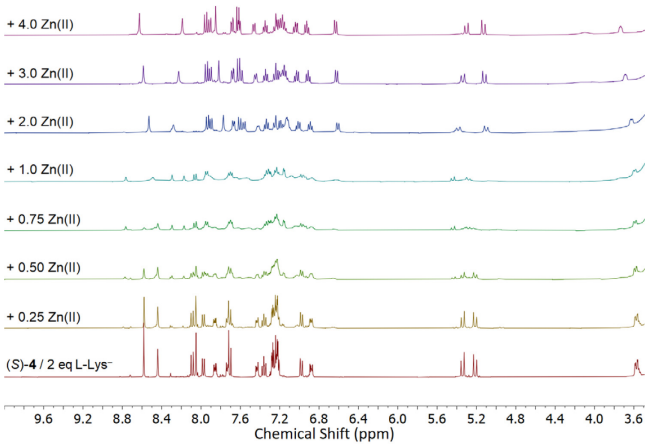

Figure 6. ^{1}H NMR spectra of (*S*)-**4** (4.0 mM) with 2 eq L-Lys$^-$ + 0 ~ 4.0 eq Zn^{2+} in DMSO-d_6. (400 MHz) (see Figure S43 for the full spectra)

^{1}H NMR studies were also conducted on the reaction of (*S*)-**4** with D-Lys$^-$ in the presence of 0 to 4.0 equiv Zn^{2+}. As detailed in Figure S54, treating the mixture of macrocycles **13** and **14**, formed from the reaction of (*S*)-**4** with 2.0 equiv of D-Lys$^-$, with 1.0 equiv of Zn^{2+} resulted in the formation of a predominant product. This product was characterized by two imine signals at δ 8.78 and δ 8.31, as verified by the HSQC spectrum (see Figure S58 in SI). Further analysis through the TOCSY spectrum (see Figure S56 in SI) revealed the transformation of the macrocyclic structures of **13** and **14** into a major product possessing a bis-D-Lys diimine structure, designated as compound **15** in Figure 7. Unlike the macrocycles discussed earlier, the two imine protons of compound **15** do not exhibit a correlation with each other in the TOCSY spectrum. TOCSY correlations were observed between the imine proton at position 1 (δ 8.78) and the two diastereotopic protons at positions 28 (δ 3.73 and 3.49), and between the imine proton at position 18 (δ 8.31) and the two diastereotopic protons at position 19 (δ 3.36 and 3.28) (see more detailed NMR assignments available in Figures S55 to S58). Addition of more than 1.0 equiv of Zn^{2+} led to the broadening of all signals. Although zinc coordination is evident as shown by the NMR analyses, it was not detected in the mass spectrum (TOF, ES+, Figure S59 in SI) which is attributed to the instability of the Zn^{2+} complex under the mass spectroscopic conditions. In this mass spectrum, a peak at m/z = 1103.445 is observed for a higher oligomeric compound **16** (as shown in Figure 7, calcd for **16**+3H: 1103.459), and a peak at m/z = 1121.465 for **16**+3H +H_2O (calcd: 1121.470).

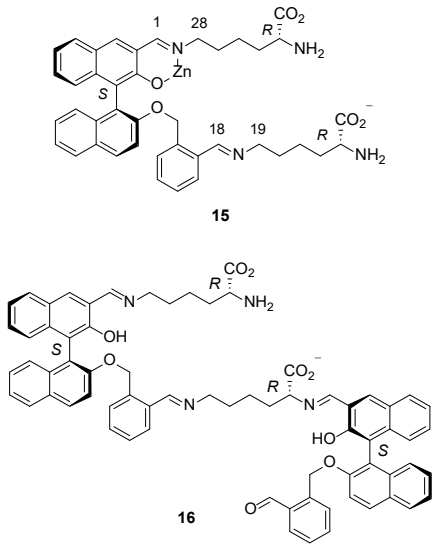

Figure 7. Structures of compounds **15** and **16**.

Further studies were conducted on the reaction of (*S*)-**4** with *rac*-Lys$^-$ in the presence of Zn^{2+}. The ^{1}H NMR spectra, shown in Figure 8 (also see Figures S60 and S61), elucidate the effects of adding 0.25 to 4.0 equiv of Zn^{2+} to the reaction mixture containing (*S*)-**4** and 2.0 equiv of *rac*-Lys$^-$ (2.0 equiv), where macrocycle **8** is formed as the major product through the regio- and enantioselective reaction with L-Lys$^-$. In the presence of 4.0 equiv of Zn^{2+}, an identical macrocyclic product, as observed in the reaction of (*S*)-**4** with L-Lys$^-$ and 4.0 equiv Zn^{2+}, was generated. Additionally, only a very small amount of the acyclic Zn-complex, formed from D-Lys$^-$, was observed in the reaction with 4.0 equiv Zn^{2+}, indicating that the presence of Zn^{2+} further enhances the regio- and enantioselectivity of the reaction between (*S*)-**4** and *rac*-Lys$^-$.

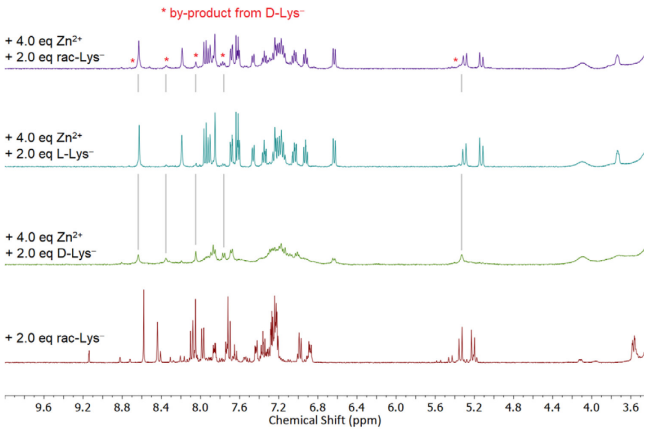

Figure 8. ^{1}H NMR spectra of (*S*)-**4** (4.0 mM) with 2 equiv D- / L- / *rac*-Lys$^-$ + 4.0 equiv Zn^{2+} in DMSO-d_6. (400 MHz)

c. Study of the Reactions of (*S*)-5 with Lys$^-$.

Compounds (*S*)-**5**, containing a *meta*-benzaldehyde unit, was prepared as a regioisomer of (*S*)-**4** and its reactions with Lys$^-$ were studied. Figure 9 gives the ^{1}H NMR spectra for the reaction of (*S*)-**5** with 0 ~ 2.0 equiv of L-Lys$^-$ in DMSO-d_6 over 6 h at room temperature. At 2.0 equiv of L-Lys$^-$, the reaction predominantly yielded a single product identified as compound **17** (Figure 10) whose macrocyclic structure was confirmed through correlations among protons 1 (δ 8.62), 18 (δ 8.20), α-proton 23 (δ 3.62), and ε-protons 19 (δ 3.53) in the ^{1}H, ^{13}C, NOESY, HSQC, TOCSY, and mass spectra, as shown in Figures S64 to S74. When the reaction involved 1.0 equiv of L-Lys$^-$, two regioisomeric macrocyclic compounds, **17** (minor) and **18** (major), were formed, as shown in Figure 9. The structure of compound **18** (Figure 10), shows imine proton signals at δ 8.81 (proton 1) and δ 8.11 (proton 18) and adjacent aliphatic signals at δ 3.96/3.42 (ε-protons 23) and δ 3.57 (α-proton 19), was established analogously to compound **17** (see Figures S75 to S83 in SI for more details).

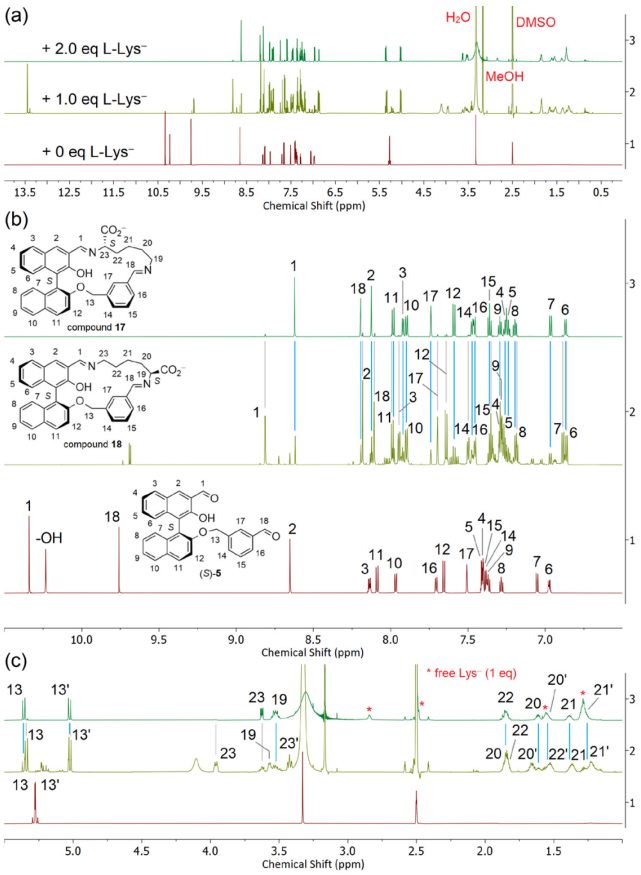

Figure 9. (a) ^{1}H NMR (800 MHz) spectra of (*S*)-**4** (4.0 mM) + 0 ~ 2.0 equiv L-Lys$^-$ in DMSO-d_6. (Reaction time: rt for 6 h). (b) and (c) zoomed regions with signal assignments. (See Figures S62 and S63 for the reaction with 0 ~ 8.0 equiv L-Lys$^-$)

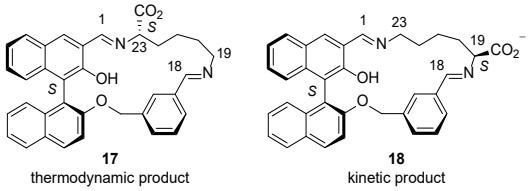

17
thermodynamic product

18
kinetic product

Figure 10. Structures of compounds **17** and **18**.

In order to understand the stability difference between the macrocycles **17** and **18**, we conducted a DFT calculation on these two anions by using Gaussian 16 program [B3LYP/6-31+G(D,P)] and the molecular modeling structures are shown in Figure 11 (see Section 10 in SI for more details). It was found that **17** is more stable than **18** by 6.4 kcal/mol. In **17**, there might be an intramolecular hydrogen bond between the carboxylic anion and the proton on the imine carbon whose acidity could be increased by the strong hydrogen bond between the o-hydroxy group and the imine nitrogen. This could increase the stability of **17** over **18** since the carboxylate group of **18** should not have significant hydrogen bonding interaction with the less acidic imine proton.

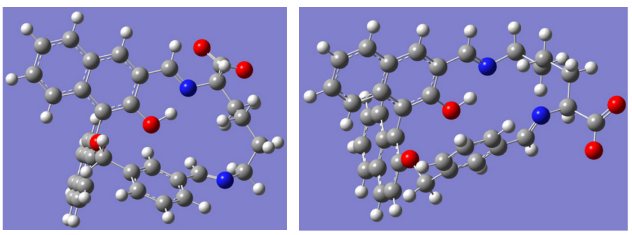

17 **18**

Figure 11. Molecular modeling structures of the two regioisomeric macrocycles **17** and **18**.

The reaction of (*S*)-**5** with the enantiomer D-Lys$^-$ was also explored. Similar to the reaction of (*S*)-**4** with D-Lys$^-$, (*S*)-**5** reacted with 1.0 equiv of D-Lys$^-$ to predominately form the macrocyclic compound **19**, while 2.0 equiv of D-Lys$^-$ resulted in both compounds **19** and **20** (Figure 12), as further elaborated in Figures S86 to S106 in SI.

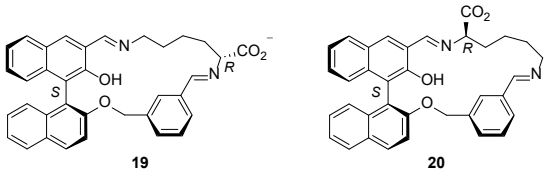

19
kinetic product

20
thermodynamic product
slightly more stable

Figure 12. Structures of compounds **19** and **20**.

Monitoring the reaction of (*S*)-**5** with 2.0 equiv of L- and D-Lys$^-$ over time (from 10 min to 6 h) via ^{1}H NMR spectroscopy yielded insights consistent with those observed for (*S*)-**4**. In the case of L-Lys$^-$, an initial 10-min reaction produced a mixture of the kinetic product **18** (major) and the thermodynamic product **17** (minor), ultimately reaching equilibrium after 6 h with a dominant yield of compound **17** (93.5%). In contrast, the reaction with D-Lys$^-$ predominantly produced the kinetic product **19** at 10 min, and upon reaching equilibrium, yielded a mixture of **19** (43.1%) and the slightly more stable product **20** (56.9%) (see Figures S84, S85, S107, and S108 in SI).

Furthermore, treating (*S*)-**5** with 2.0 equiv of *rac*-Lys$^-$ resulted in the formation of the two kinetic products **18** and **19** in approximately a 1:1 ratio initially within 10 min, as shown in the ^{1}H NMR spectra in Figure S109 and S110 in SI. Upon reaching equilibrium after 20 h, the reaction demonstrated both regio- and enantioselectivity, predominantly yielding the thermodynamically more stable product **17** (67%) as the major product. The DFT calculation of **20** by using Gaussian 16 program [B3LYP/6-31+G(D,P)] also shows that **20** is less stable than **17** by 1.2 kcal/mol (see Section 10 in SI for more details).

Based on the above observations, it is concluded that the reaction dynamics of (*S*)-**5** with L- and D-Lys$^-$ are highly similar to those of (*S*)-**4**, following a comparable mechanism as outlined in Scheme 2.

Compound **17**, formed from the reaction of (*S*)-**5** with 2.0 equiv of L-Lys$^-$, was subsequently treated with 0 to 4.0 equiv of Zn^{2+}, and the reactions were monitored via ^{1}H NMR spectroscopy. As shown in Figure 13, the addition of 1.0 equiv of Zn^{2+} led to the broad signals, with the two imine signals of compound **17** coalescing at δ 8.44. This suggests that the coordination between compound **17** and 1 equiv of Zn^{2+} may facilitate the formation of dynamic interconverting structures.

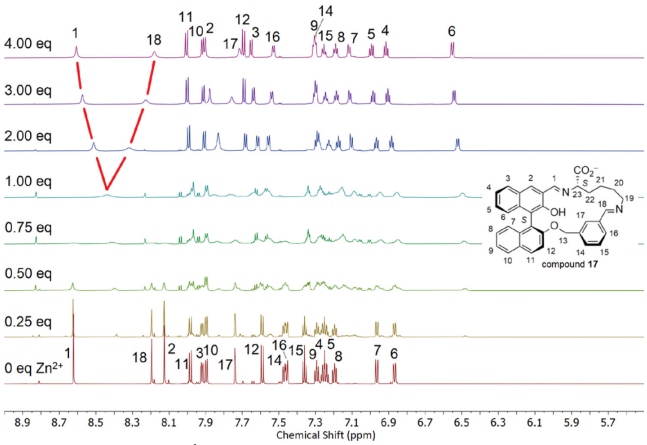

Figure 13. Partial ^{1}H NMR (800 MHz) spectra of (*S*)-**5** (4.0 mM) + 2.0 equiv L-Lys$^-$ with 0 ~ 4.0 equiv Zn^{2+} in DMSO-d_6. (see Figures S111 and S112 for the full spectra)

Scheme 3 shows the proposed interconverting structures as compounds **21** and **22**. (DFT calculations were conducted on **21** and **22** by using Gaussian 16 program [B3LYP/6-31+G(D,P)], see Section 10 in SI for more details) It was found that **22** is more stable than **21** by 10.0 kcal/mol. Upon the addition of more than 1.0 equiv of Zn^{2+}, the previously merged imine signal at δ 8.44 separates into two distinct signals, which stabilize at δ 8.61 and 8.18 with 4.0 equiv of Zn^{2+}, as shown in Figures S113 to S120. TOCSY correlations between the imine protons 1 and 18, ε-protons 19 and α-proton 23 confirm that the macrocyclic structure of compound **17** is preserved after its interaction with Zn^{2+} (see Figures S1115 and S119). The excess Zn^{2+} appears to saturate the coordination sites of compound **17**, resulting in sharp signals for the final **17**+4Zn^{2+} complex. The TOF mass spectrum (ES+) of macrocycle **17** in the presence of excess Zn^{2+} reveals only the signal for the mono-Zn(II)-coordinated species at m/z = 623.1523 (calculated for **21** + H + H_2O: 623.1524), as illustrated in Figures S121 and S122. Signals indicative of multiple Zn^{2+} coordination were not detected, likely due to the instability of additional Zn^{2+} coordination under mass spectrometric conditions. Despite attempts to crystallize the **17**+4Zn^{2+} complex for X-ray diffraction analysis, it was isolated only as powders, incorporating various solvent molecules, as detailed in Figures S123 and S124 in SI.

Scheme 3. Proposed interconversion of two macrocyclic Zn^{2+} complexes **21** and **22**.

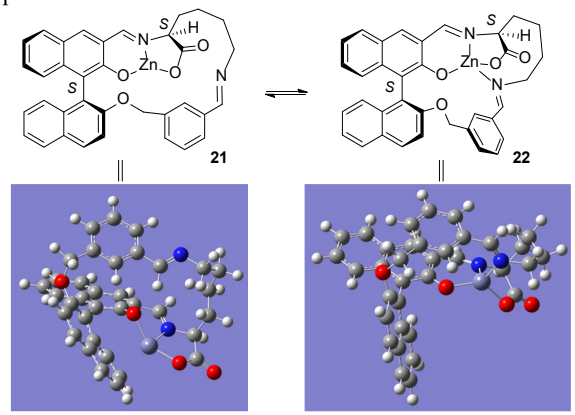

Additions of 0.25 ~ 4.0 equiv Zn^{2+} to the mixture of compounds **19** (43.1%) and **20** (56.9%), formed from the reaction of (*S*)-**5** with 2.0 equiv D-Lys$^-$, were also monitored by ^{1}H NMR spectroscopy. Similar to the reaction of Zn^{2+} with (*S*)-**4**+D-Lys$^-$, the addition of 1.0 equiv of Zn^{2+} yielded a ring-opened structure, designated as compound **23** (as shown in Figure 14, see Figures S125 to S136 in SI for more details). When more than 1.0 equiv Zn^{2+} was introduced, similar to that with (*S*)-**4**, all ^{1}H NMR signals became broad, indicating the formation of complex Zn-complexes such as oligomers and polymers. The TOF Mass (ES$^-$) spectrum of the reaction mixture of (*S*)-**5** + 2.0 equiv D-Lys$^-$ + 1.0 equiv Zn^{2+} in DMSO-d_6 shows the base peak at m/z = 659.147 for **23** (calcd for **23**−NH_2−H_2O−C_4H_8: 659.140); a peak at m/z = 1045.279 in the above spectrum is observed for a higher oligomeric zinc complex **24** (as shown in Figure 14, calcd for **24**+H−$CH_2C_6H_4CHO$: 1045.316), and a peak at m/z = 1119.452 for **24**−Zn+2H+H_2O (calcd: 1119.455) (Figure S137 in SI). The formation of compound **23** indicates that the macrocyclic compounds **19** and **20**, generated from the reaction of (*S*)-**5** with D-Lys$^-$, are not stable in the presence of Zn^{2+}, leading to the ring-opened products.

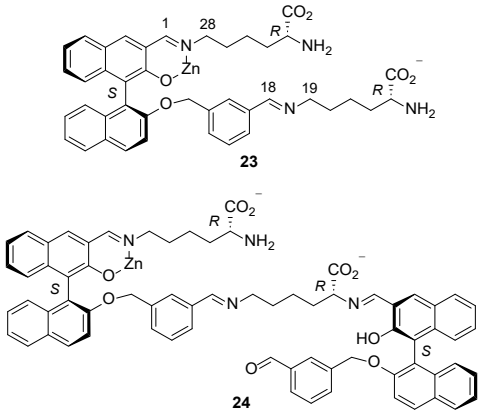

Figure 14. Structures of compounds **23** and **24**.

Subsequent studies were conducted on the reaction of (*S*)-**5** with *rac*-Lys$^-$ in the presence of Zn^{2+}. Figure 15 shows the ^{1}H NMR spectra following the incremental addition of Zn^{2+} (from 0 to 4.0 equiv) to a mixture of (*S*)-**5** and *rac*-Lys$^-$ (2.0 equiv), where the macrocycle **17** is identified as the predominant product generated from the regio- and enantioselective reaction between (*S*)-**5** and L-Lys$^-$. Upon introduction of 4.0 equiv of Zn^{2+}, the spectra reveal the formation of an identical final macrocyclic product, as observed in the reaction of (*S*)-**5** with L-Lys$^-$ and 4.0 equivalents of Zn^{2+}. It is noteworthy that, in contrast to the reactions involving (*S*)-**4** (see Figure 8), no products attributable to the reaction between (*S*)-**5** and D-Lys$^-$ in the presence of Zn^{2+} were observed. That is, (*S*)-**5** exhibits higher enantioselectivity than (*S*)-**4** in the reaction with Lys$^-$ in the presence of Zn^{2+}.

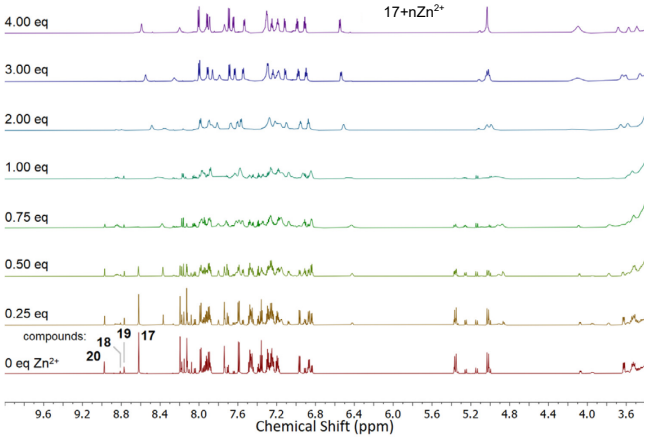

Figure 15. ^{1}H NMR (800 MHz) spectra of (*S*)-**5** (4.0 mM) + 2.0 equiv *rac*-Lys$^-$ with 0 ~ 4.0 equiv Zn^{2+} in DMSO-d_6. (see Figure S138 for more details).

The above experiment demonstrates a significant enhancement in the enantioselectivity for the reaction between (*S*)-**5** and Lys⁻ upon addition of Zn^{2+}. Specifically, in the presence of Zn^{2+}, (*S*)-**5** selectively reacts with L-Lys⁻ in a 1:1 mixture of L- and D-Lys⁻, leading to the formation of one single macrocyclic Zn^{2+} complex with high regio- and enantioselectivity.

d. Study of the Reactions of (*S*)-6 with Lys⁻

The reaction of another regioisomer (*S*)-**6**, containing a *para*-benzaldehyde unit, with Lys⁻ was studied. As the ^{1}H NMR spectra in Figure 16 show, when (*S*)-**6** was treated with 1.0 equiv L-Lys⁻, all of the salicylaldehyde signal at δ 10.34 disappeared with the appearance of several new signals for the OH protons at δ > 12 which are much more downfield-shifted than the OH signal of (*S*)-**6** at δ 10.23. This indicates the formation of a mixture of imine products with stronger intramolecular hydrogen bonds. These products could be regioisomeric macrocycles and oligomers from the condensation of the unsymmetric dialdehyde with the unsymmetric diamine. The TOCSY, HSQC, and HRMS spectra are available in Figures S144 to S146 in SI for the reaction with 1.0 equiv L-Lys⁻. In the presence of 2.0 equiv L-Lys⁻, the ^{1}H NMR spectrum became much simpler. The disappearance the signals at δ > 12 can be attributed to fast exchanges of the OH protons in the presence of the excess amine. On the basis of TOCSY and HSQC spectra (Figures S140 to S142 in SI), the major imine signal at δ 8.69 can be assigned to the proton 1 of the macrocycle **25** (as shown in Figure 17). This proton has a cross peak with an imine proton signal (proton 16) at δ 8.10, and the α-proton signal (proton 21) of the lysine unit at δ 3.64 in the TOCSY spectrum. The structures of the other imine products such as the macrocycle **26** and the acyclic compounds like **27** (Figure 17) cannot be unambiguously assigned due to signal overlaps or low intensity. When (*S*)-**6** was treated with 4.0 equiv L-Lys⁻, the signal at δ 8.75 became more intense. It is proposed that this might be due to the conversion of the macrocycles such as **25** to the acyclic imine products like **27** in the presence of greater excess of the chiral diamine. That is, the macrocycle **25** may be less stable than **8** and **17** where no such conversion was observed when 4 ~ 8 equiv L-Lys⁻ were added to react with (*S*)-**4** and (*S*)-**5** (Figures S15 and S63 in SI).

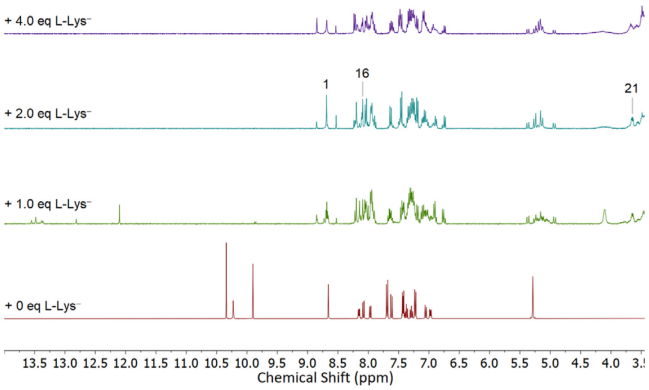

Figure 16. ^{1}H NMR spectra of (*S*)-**6** (4 mM) + 0 ~ 4.0 eq L-Lys⁻ in DMSO-d_6 (400 MHz) (see Figure S139 for the full spectra in SI).

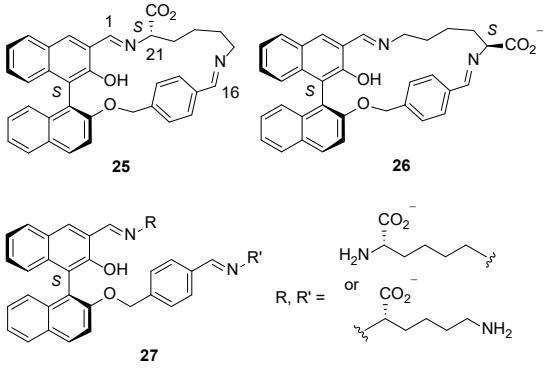

Figure 17. Structures of compounds **25**, **26**, and **27**.

When (*S*)-**6** was treated with 1.0 or 2.0 equiv D-Lys⁻, the reaction was more complex as shown by the ^{1}H NMR spectra in Figure 18 (see Figure S147 in SI for full spectra). The TOCSY and HSQC spectra (Figures S148, S149, S151, and S152 in SI) indicate the formation of both cyclic and acyclic products. It demonstrates that the reaction with D-Lys⁻ is much less selective than with L-Lys⁻, leading to the formation of a greater product mixture (additional HRMS spectra with 1.0 and 2.0 equiv D-Lys⁻ are available in Figures S150 and S153). Further addition of D-Lys⁻ to 4.0 equiv generated a major product with a proposed acyclic structure of **28** on the basis of the TOCSY and HSQC spectra (see Figures S154 to S156 in SI, HRMS spectrum is available in Figure S157). In the TOCSY spectrum (Figure S155), the imine proton signal 1 at δ 8.86 is correlated with the two diastereotopic protons 26 at δ 3.69 and 3.59, and the imine proton 16 at δ 8.21 is correlated with the two protons 17 at δ 3.49. This demonstrates that the macrocycles generated from the reaction of (*S*)-**6** with D-Lys⁻ should be less stable than compound **25** formed from L-Lys⁻ and they react with excess D-Lys⁻ to form the acyclic product **28** as the major product. When (*S*)-**6** was treated with 4.0 equiv L-Lys⁻, there might be an increased formation of an acyclic imine compound similar to **28** but the macrocycle **25** was still the major product (see Figures 16 and S139).

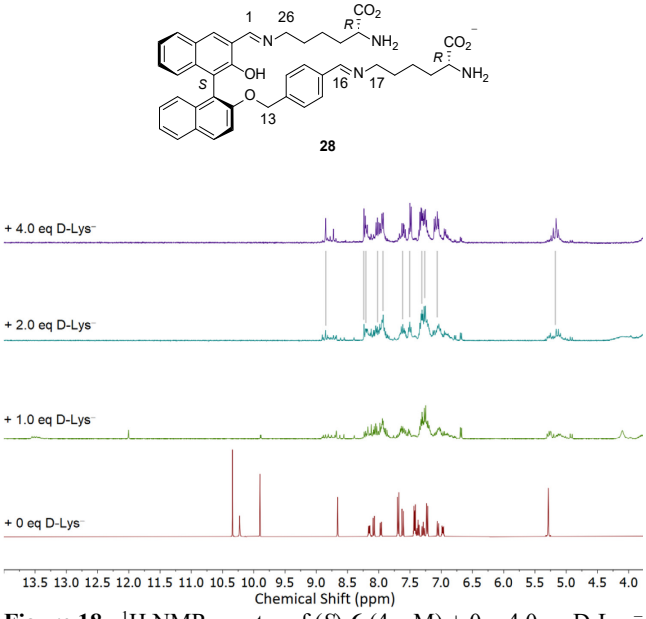

Figure 18. ^{1}H NMR spectra of (*S*)-**6** (4 mM) + 0 ~ 4.0 eq D-Lys⁻ in DMSO-d_6. (400 MHz) (see Figure S147 for the full spectra in SI).

When (*S*)-**6** was treated with 2 equiv *rac*-Lys⁻, the reaction products were predominately those generated from the reaction of

(*S*)-**6** with L-Lys$^-$, rather than with D-Lys$^-$, as shown in Figure 19 (see Figure S158 in SI for full spectra). This demonstrates that the reaction of (*S*)-**6** with Lys$^-$ has good enantioselectivity.

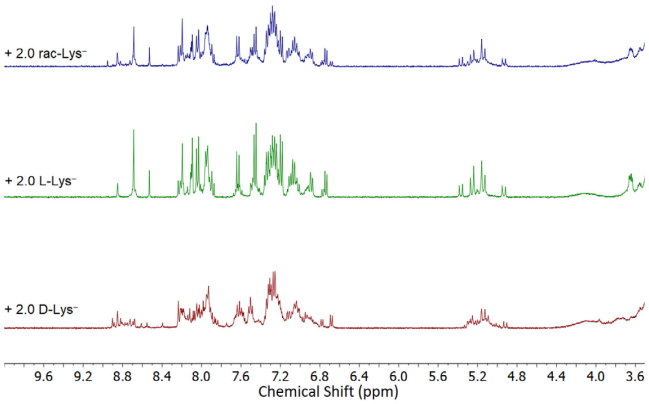

Figure 19. ^{1}H NMR spectra of (*S*)-**6** (4.0 mM) + D-/L-/*rac*-Lys$^-$ in DMSO-d_6. (400 MHz) (see Figure S158 for the full spectra in SI).

When (*S*)-**6** + 2.0 equiv L-Lys$^-$ was treated with 4.0 equiv Zn^{2+}, the ^{1}H NMR spectrum shows the formation of a major imine + Zn^{2+} product together with several minor products (Figures 20 and S160). In the HSQC spectrum (Figure S162 in SI), no ^{13}C NMR signal around δ 70 is observed for the Lys α-carbon of the moiety -CH=N-<u>CH</u>(CO_2^-)- and only cross signals with the ^{13}C NMR signals of the units like -CH=N-<u>CH_2</u>- at δ 53-60 are observed (The TOCSY spectrum is also available in Figure S161). This indicates the formation of an acyclic imine + Zn^{2+} complex like **29**+nZn^{2+} (Figure 21). The mass spectrum in Figure S163 (TOF, ES+) gives a barely observed signal at m/z = 750.23 for **29**+Zn (calcd: 750.24). The following significant signals are observed: a peak at m/z = 688.30 for **29**+2H (calcd: 688.33), a peak at m/z = 623.15 for **30**+Zn (calcd: 623.15), and a peak at m/z = 579.11 for **30**+Zn-CO_2 (calcd: 579.16). This indicates that the macrocycles formed from the reaction of (*S*)-**6** with L-Lys$^-$ were not stable in the presence of Zn^{2+}, leading to the ring-opened reaction and forming acyclic imine products.

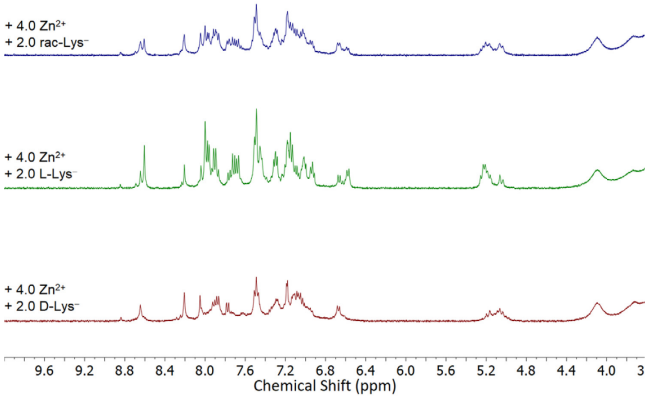

Figure 20. ^{1}H NMR spectra of (*S*)-**6** (4.0 mM) with 2 equiv D- / L- / *rac*-Lys$^-$ + 4.0 equiv Zn^{2+} in DMSO-d_6. (400 MHz) (See Figure S159 for more details).

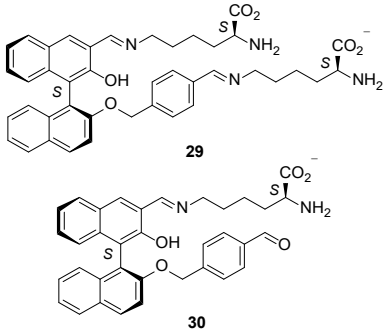

Figure 21. Structures of compounds **29** and **30**.

When (*S*)-**6** + 2.0 equiv D-Lys$^-$ was treated with 4.0 equiv Zn^{2+}, the ^{1}H NMR spectrum shows the conversion of the complex mixture to a major imine+Zn^{2+} product and a few minor products (Figures 20 and S164). The TOCSY and HSQC spectra give observations similar to those observed for the treatment of (*S*)-**6** + 2.0 equiv L-Lys$^-$ with 4.0 equiv Zn^{2+} (Figures S165 and S166 in SI). Thus, the formation of the acyclic product **28**+nZn^{2+} is proposed. This complex might be too unstable under the mass analysis conditions to give identifiable signals. The major signal at m/z 561.2389 in the mass spectrum is attributed to the partially hydrolyzed product **31**+2H (calcd: 561.2395) (Figure S167 in SI).

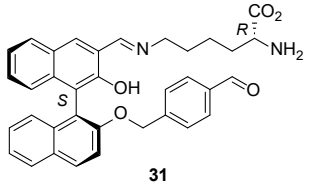

When (*S*)-**6** + 2.0 equiv *rac*-Lys$^-$ was treated with 4.0 equiv Zn^{2+}, the ^{1}H NMR spectrum indicates the formation of a mixture of the acyclic complex **28**+nZn^{2+}, generated from L-Lys$^-$, and other complexes (Figures 20 and S159).

The above study demonstrates that the reactions of (*S*)-**6** with Lys$^-$ are less selective than the reactions of (*S*)-**4** and (*S*)-**5** with Lys$^-$, giving more products in the mixture. Macrocycles, such as **25**, are less stable and can be easily converted to the acyclic products, such as **28** and **29**, especially in the presence of Zn^{2+}. This indicates that the *para*-benzaldehyde unit of (*S*)-**6** might have introduced more ring strain for the corresponding macrocycles than the *ortho*- and *meta*-benzaldehyde units of (*S*)-**4** and (*S*)-**5**. Nevertheless, (*S*)-**6** still exhibited good enantioselectivity when treated with *rac*-Lys$^-$, favoring the reaction with L-Lys$^-$ over D-Lys$^-$.

e. Comparison of the Macrocycles from the Reactions of the Three Regioiosmeric Chiral Dialdehydes with L- and D-Lys$^-$.

In order to gain a better understanding on the difference in the reactions of the three isomeric compounds with Lys, we conducted DFT calculations [Gaussian 16W, B3LYP, 6-31+G(D,P)] on the macrocycles formed from the reaction of (*S*)-**4**, (*S*)-**5** and (*S*)-**6** with L-Lys$^-$ (Figure 22) (See Section 10 in SI for detailed information). It was found that the macrocycle **17** formed from (*S*)-**5**+L-Lys$^-$ is the most stable one. The macrocycle **8** formed from (*S*)-**4**+L-Lys$^-$ is less stable than **17** by 3.4 kcal/mol. The macrocycle **25** formed from (*S*)-**6**+L-Lys$^-$ is the least stable one and it is less stable than **17** by 5.4 kcal/mol. Thus, the *para*-benzaldehyde unit of (*S*)-**6** might have led to a macrocycle with more ring strain than the other two regioisomers. This is consistent with the observed higher stability of **8** and **17** than **25** when treated with 4 ~ 8 equiv L-Lys$^-$.

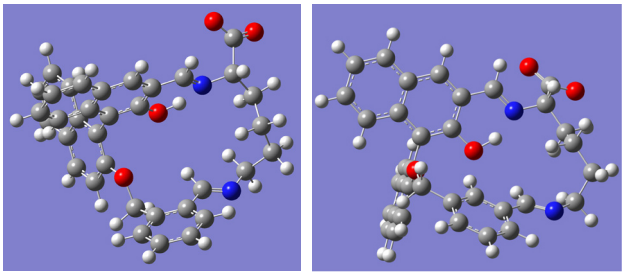

8 [(*S*)-**4**+L-Lys$^-$]
3.4 kcal/mol

17 [(*S*)-**5**+L-Lys$^-$]
0 kcal/mol

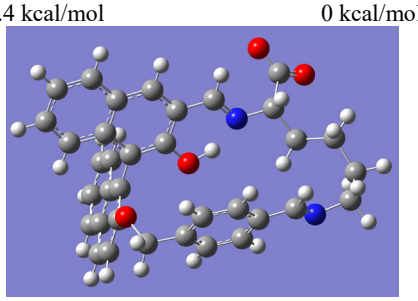

25 [(*S*)-**6**+L-Lys$^-$]
5.4 kcal/mol

Figure 22. The molecular modeling structures of macrocycles **8**, **17**, and **25** and the calculated relative energies.

All the mass spectra (TOF, ES+) of the reaction mixtures of (*S*)-**4**, (*S*)-**5**, and (*S*)-**6** with 2 equiv L-/D-Lys$^-$ display two peaks at m/z = 543.228 and 561.238 corresponding to the macrocycle+2H and the macrocycle+2H+H_2O respectively (see Figures S20, S38, S74, S106, S143, and S153). Since the ^{1}H NMR spectra of the samples used for the mass analyses showed the complete disappearance of both aldehyde signals, the signals at m/z = 561.238 are believed to be produced from the ring-opening of the macrocycles by reaction with one equivalent water under the mass analysis conditions (see mass spectrometry conditions in the experimental section) to form the monoaldehydes such as **10, 11**, and **30**. The intensity ratios of the peak at m/z = 543.228 (I_{543}) to that at m/z = 561.238 (I_{561}) are listed in Table S1. It is proposed that macrocycles with higher intensity ratios might be more stable and more resistant to the partial hydrolysis under the mass analysis conditions than those macrocycles with lower intensity ratios. Thus, the macrocycle **17**, generated from the reaction of (*S*)-**5** with 2 equiv L-Lys$^-$, should be the most stable one with a ratio of 7.5, and those generated from (*S*)-**6**+L-/D-Lys$^-$ with ratios of around 0.02 are considered to be the least stable ones. This hypothesis is consistent with the calculated relative energies of the macrocycles formed from (*S*)-**4**, (*S*)-**5**, and (*S*)-**6** with L-Lys$^-$ as shown in Figure 22. It should be noted that the intensity ratios obtained from high-resolution mass spectrometry are more qualitative than quantitative in nature, and they are used only to roughly reflect the relative stability among the different structures.

f. Fluorescence Response of (*S*)-4, (*S*)-5, and (*S*)-6 toward Lys and Other Amino Acids in the Presence of Zn^{2+}.

The C_2 symmetric chiral dialdehyde (*S*)-**1** in combination with Zn^{2+} exhibited enantioselective fluorescent responses toward a number of functional chiral amines including amino acids.[11] Because fluorescent probes are potentially useful for the analysis of biologically significant amino acids, we studied the fluorescent responses of compounds (*S*)-**4**, (*S*)-**5**, and (*S*)-**6** toward Lys and other amino acids in the presence of Zn^{2+}.

Figure 23 gives the fluorescence spectra of (*S*)-**4** ~ (*S*)-**6** with D- and L-Lys (10 equiv, BICINE buffer, pH = 8.4) in the presence of $Zn(OAc)_2$ (2.0 equiv). It shows that L-Lys significantly enhanced the fluorescence of all of these compounds at λ_{emi} = 550 nm (λ_{exc} = 440 nm) with the highest enhancement by (*S*)-**5** then (*S*)-**4** and the lowest by (*S*)-**6**. The fluorescence intensity of (*S*)-**5** was increased by L-Lys to 317 folds. (*S*)-**4** and (*S*)-**6** exhibit only 38.0% and 9.8%, respectively, of the intensity of (*S*)-**5** with L-Lys. D-Lys induced much weaker fluorescence responses of these compounds. With 10 equiv of Lys, the enantioselective fluorescence enhancement ratio [*ef* = $(I_L–I_0)/(I_D–I_0)$. I_0: the fluorescence intensity in the absence of L- and D-lysine] was found to be 7.4 for (*S*)-**4**, 16.9 for (*S*)-**5**, and 2.4 for (*S*)-**6**. Thus, (*S*)-**5** is the most sensitive as well as enantioselective fluorescent probe for Lys among these three compounds.

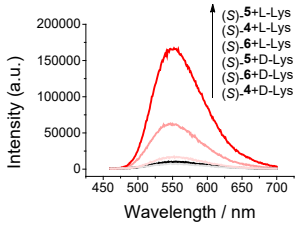

Figure 23. Fluorescence spectra of (*S*)-**4**, (*S*)-**5**, or (*S*)-**6** (0.5 mM) + $Zn(OAc)_2$ (2.0 equiv) with D- and L-Lys (10 equiv) (λ_{exc} = 440 nm, slit: 1/1 nm. Solvent: CH_3CN/H_2O = 1/1 with 12.5 mM pH 8.4 buffer).

The highest fluorescence enhancement of (*S*)-**5** by L-Lys in the presence of Zn^{2+} could be attributed to the ability of (*S*)-**5** to form the most stable macrocycle with L-Lys among the three regioiosomeric dialdehyde probes. Coordination of the macrocycle with Zn^{2+} might generate the most structurally rigid complex, which can restrict the relative rotation of the two naphthyl units and inhibit the intramolecular excited state proton transfer of the hydroxy group, and the excited state isomerization of the imines, leading to the greatly enhanced fluorescence. Compound (*S*)-**6** shows the lowest fluorescence enhancement with L-Lys because of the instability of its macrocyclic product especially in the presence of Zn^{2+}, which should generate the structurally flexible acyclic compounds of weak emission.

We studied the fluorescence responses of (*S*)-**4**, (*S*)-**5**, and (*S*)-**6** in the presence of Zn^{2+} towards 17 enantiomeric pairs of common amino acids (including Lys). Under the same conditions, as illustrated in Figure 24, (*S*)-**5** exhibited the most pronounced chemo- and enantioselective fluorescence responses. Specifically, in the presence of Zn^{2+}, only L-Lys can significantly enhance the fluorescence of (*S*)-**5** at λ_{em} = 550 nm, while D-Lys and all other amino acid enantiomers cannot (see Figures S168, S175, and S183 for full spectra). The chemoselective fluorescence responses of (*S*)-**4** and (*S*)-**5** toward L-Lys can be attributed to lysine's unique diamino structure, which enables the formation of the more stable macrocycles **8** and **17**; other amino acids cannot form macrocyclic products with (*S*)-**4** and (*S*)-**5** and thus cannot give significant fluorescence enhancement.

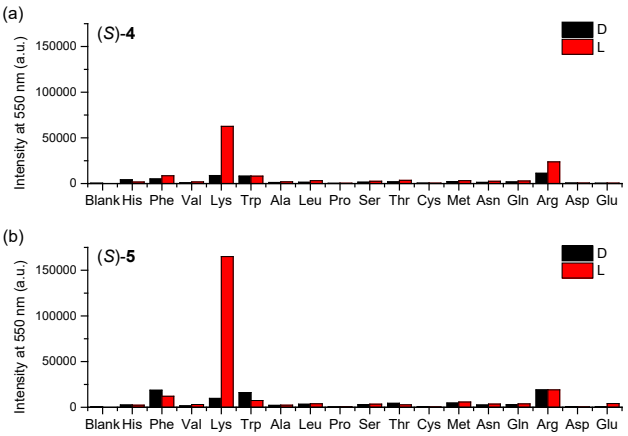

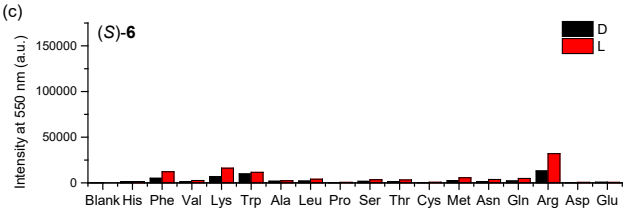

Figure 24. Fluorescence intensity at 550 nm of (a) (*S*)-**4**, (b) (*S*)-**5**, and (c) (*S*)-**6** (0.5 mM) + $Zn(OAc)_2$ (2.0 equiv) with 17 pairs of amino acid enantiomers (10 equiv) (λ_{exc} = 440 nm, slit: 1/1 nm. Solvent: CH_3CN/H_2O = 1/1 with 12.5 mM pH 8.4 buffer)

The fluorescence responses of (*S*)-**5** toward Lys were further examined in detail because of its highest chemoselectivity and enantioselectivity among the three unsymmetric chiral dialdehydes [see Figures S169 to S174 and S184 for additional fluorescence studies on (*S*)-**4** and (*S*)-**6**]. As shown in Figure 25a, (*S*)-**5** exhibits no fluorescence at λ_{emi} = 550 nm, and the presence of Zn^{2+} does not affect the fluorescence properties of (*S*)-**5**. However, when (*S*)-**5** was treated with Lys, only L-Lys in combination with Zn^{2+} significantly enhanced the fluorescence signal at 550 nm, but L-Lys without Zn^{2+} or D-Lys with or without Zn^{2+} gave only very weak emission (Figure 25a-c). Figure 25d shows that increasing L-Lys concentrations leads to significant enhancement in fluorescence intensity initially, which stabilizes once [L-Lys] exceeds 13 equiv. In contrast, D-lysine results in only minor changes in fluorescence throughout the entire concentration range (0–20 equiv). The detection limit (LOD) for L-Lys with compound (*S*)-**5** was found to be 1.41×10^{-7} M, as determined in Figure S180.

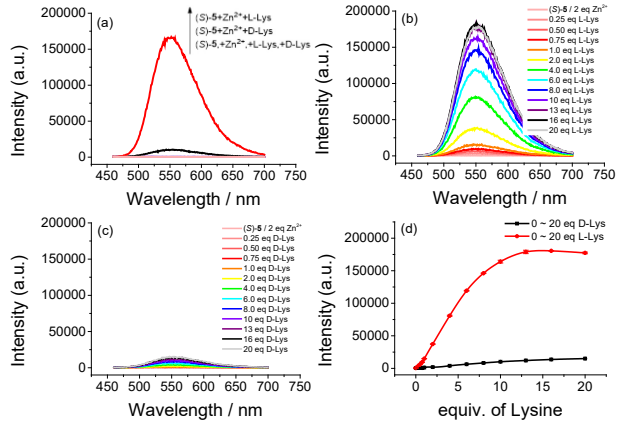

Figure 25. Fluorescence spectra of (*S*)-**5** (0.5 mM) + $Zn(OAc)_2$ (2.0 equiv) with (a) D- and L-Lys (10.0 equiv), (b) L-Lys (0 – 20 equiv), and (c) D-Lys (0 – 20 equiv). (d) Fluorescence intensity at 550 nm *versus* the equivalence of D- and L-Lys (error bars from three independent experiments. λ_{exc} = 440 nm. Slit: 1/1 nm. Solvent: CH_3CN/H_2O = 1/1 with 12.5 mM pH 8.4 buffer) (see Figures S176 to S179 for excitation spectra, UV-vis spectra, and fluorescence experiment procedure screening).

The enantiomer of (*S*)-**5**, compound (*R*)-**5**, was synthesized from (*R*)-**7**, and its fluorescence response toward D- and L-lysine was studied under the same conditions. As shown in Figure S181 in SI, a mirror-image relation was observed between the fluorescence responses of (*R*)-**5** and (*S*)-**5** toward the enantiomers of Lys at 550 nm, which confirms the inherent chiral recognition process.

The interaction of both (*S*)-**5** and (*R*)-**5** with Lys at various enantiomeric compositions was studied. In Figure 26, the fluorescence responses of (*S*)-**5** and (*R*)-**5** at 550 nm are plotted against the enantiomeric excess [ee = ([D] – [L]) / ([D] + [L]) %] of Lys, demonstrating a mirror-image relationship between the fluorescence responses of this enantiomeric probe pair. These plots can be utilized to determine the enantiomeric composition of Lys at the concentration.

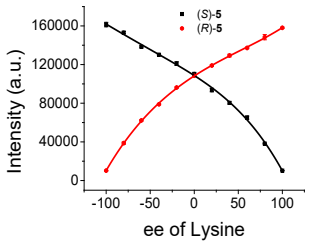

Figure 26. Fluorescence intensity of (*S*)-**5** or (*R*)-**5** (0.5 mM) + $Zn(OAc)_2$ (2.0 equiv) at 550 nm *versus* the ee of Lys (10.0 equiv) (error bars from three independent experiments. λ_{exc} = 440 nm, slit: 1/1 nm. CH_3CN/H_2O = 1/1 with 12.5 mM pH 8.4 buffer) (see Figure S181 in SI for the fluorescence spectra)

We also investigated the fluorescence responses of (*S*)-**5** + Zn^{2+} towards Lys when other amino acids were present. As illustrated in Figure 27, the addition of most amino acids did not significantly affect the fluorescence response of (*S*)-**5** towards L-Lys, except that the presence of histidine and cysteine inhibited fluorescence enhancement, and the presence of arginine caused further fluorescence enhancement.

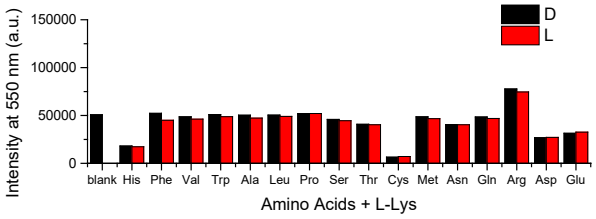

Figure 27. Fluorescence intensity of (*S*)-**5** (0.50 mM) + $Zn(OAc)_2$ (2.0 equiv) with L-Lys (3.0 equiv) + one of 16 common amino acids and their enantiomers (3.0 equiv) at 550 nm. (λ_{exc} = 440 nm. Slit: 1/1 nm. Solvent: CH_3CN / water = 1 / 1 with 12.5 mM pH 8.4 phosphate buffer). (see Figure S182 for the spectra)

L-Lys is an essential amino acid for human health and it plays roles in protein synthesis, mineral nutrient uptake, and fatty acid metabolism.[12] Its enantiomer, D-Lys, holds significance in various bacterial processes and serves as a valuable component in the development of antimicrobial and antitubercular medications.[13,14] Extensive progress has been made in the development of fluorescent probes for the detection of amino acids[15] including Lys[16] because the fluorescence-based method offers advantages such as easily available instrumentation, high sensitivity, and rapid analysis. However, very few probes are able to conduct both chemoselective as well as enantioselective discrimination of Lys.[17] The high chemoselectivity and enantioseletivity of compounds (*S*)-**5** and (*R*)-**5** in the fluorescent recognition of Lys make them potentially useful for the detection of the enantiomers of this amino acid.

g. Conclusion

Three regioisomeric BINOL-based chiral dialdehydes, (*S*)-**4**, (*S*)-**5**, and (*S*)-**6**, have been synthesized, and their reactions with both enantiomers of Lys have been investigated. It has been found that compounds (*S*)-**4** and (*S*)-**5**, containing ortho- and meta-benzaldehyde units respectively, show high regioselectivity and enantioselectivity in the formation of macrocycles with Lys. They are the first examples of regioselective as well as enantioselective reactions of an unsymmetric chiral dialdehyde with an unsymmetric chiral diamine to generate unsymmetric chiral macrocycles. These reactions exhibit further enhanced selectivity

in the presence of Zn^{2+}. However, compound (*S*)-**6** containing a para-benzaldehyde unit shows lower selectivity in the reaction with Lys which can be attributed to the lower stability of the corresponding macrocycles. Both (*S*)-**4** and (*S*)-**5**, in the presence of Zn^{2+}, exhibit chemoselective as well as enantioselective fluorescent enhancement upon interaction with Lys with (*S*)-**5** giving greater enhancement. They are potentially useful for fluorescent analysis of this amino acid.

Experiment Section

General Data. The commercially available chemicals were from Sigma Aldrich Chemical Co., Alfa Aesar, or TCI America. 4-(Bromomethyl) benzaldehyde was purchased from Ambeed and used directly. All solvents used in the fluorescence measurements were HPLC or spectroscopic grades. NMR spectra were recorded on a Varian-600 MHz spectrometer, a Bruker-400 MHz spectrometer, a Bruker-600 MHz spectrometer, and a Burker-800 MHz spectrometer. Optical rotation measurements were conducted on a Jasco P-2000 digital polarimeter. Chemical shifts for ^{1}H NMR spectra were recorded in parts per million relative to the solvent signals at 7.26 ppm for $CDCl_3$ and 2.50 ppm for DMSO-d_6. Chemical shifts for ^{13}C NMR were recorded relative to the centerline of a triplet at 77.16 ppm for $CDCl_3$ and a septet at 39.52 ppm for DMSO-d_6. Mass spectroscopic analyses were conducted by the University of Illinois at Urbana-Champaign Mass Spectrometry Facility. Steady-state fluorescence spectra were recorded with a Horiba FluoroMax-4 spectrofluorometer. UV-Vis spectra were measured by Shimadzu UV-2600 UV-Vis spectrometer. Elemental analyses were conducted with a Perkin Elmer 2400 CHNS/O Series II.

Synthesis and Characterization of (*S*)-4. Under nitrogen, (*S*)-**7**[10] (1.00 g, 2.79 mmol), 2-bromomethylbenzaldehyde (1.11 g, 2.0 equiv) and K_2CO_3 (3.08 g, 8.0 equiv) were placed in a three necked round bottom flask. Acetonitrile (25 mL) was then added, and the solution was bubbled with N_2 for 15 min. After the reaction flask was heated at reflux in an oil bath with stirring overnight, it was cooled to room temperature, and the solvent was removed by roto-evaporation. The mixture was then dissolved in CH_2Cl_2 (50 mL) and washed with NaCl (saturated solution, 3 × 50 mL). After the organic phase was dried with Na_2SO_4 and filtered, the solvent was removed. The resulting crude product was used directly for the next step without further purification. The crude product was dissolved in THF under N_2 (5 mL), and HCl (6.0 M, 30 mL) was added to produce a yellow solid. More THF was added until the solid was dissolved. After the solution was stirred overnight at room temperature, Na_2CO_3 (sat.) was slowly added with stirring to neutralize the acid. After the removal of THF, CH_2Cl_2 (50 mL) was added to dissolve the mixture. The organic phase was washed with NaCl (sat., 55 mL) and dried with Na_2SO_4. After filtration, CH_2Cl_2 was removed by rotary-evaporation, and the crude product was purified by column chromatography on silica gel, eluted with CH_2Cl_2 to give (*S*)-**4** as a yellow solid in 99.3% yield (1.20 g). ^{1}H NMR (600 MHz, $CDCl_3$) δ 10.44 (s, 1H), 10.19 (s, 1H), 9.98 (s, 1H), 8.32 (s, 1H), 7.99 (d, 2H), 7.90 (d, 1H), 7.71 (d, 1H), 7.50 (d, 1H), 7.40-7.32 (m, 4H), 7.28 (t, 2H), 7.25-7.17 (m, 2H), 7.14 (d, 1H), 5.59 (d, 1H), 5.52 (d, 1H). ^{13}C{^{1}H} NMR (200 MHz, $CDCl_3$) δ 196.9, 193.1, 154.0, 153.6, 140.0, 138.02, 138.00, 133.9, 133.8, 133.6, 132.8, 130.5, 130.4, 129.8, 129.7, 128.4, 127.7, 127.6, 127.4, 126.9, 125.5, 125.1, 124.4, 124.2, 122.2, 118.7, 118.4, 115.5, 69.0. HRMS (ESI-TOF): m/z calcd for $C_{29}H_{19}O_4$ $[M-H]^-$: 431.1288, found 431.1278. $[\alpha]_D^{24} = -116.7$ (c = 0.2, CH_2Cl_2), mp: 125–128°C.

Synthesis and Characterization of (*S*)-5. (*S*)-**5** was synthesized from the reaction of (*S*)-**7** with 3-bromomethyl-benzaldehyde by using the same procedure as the preparation of (*S*)-**4**. Yellow solid, 98.8%, 1.19 g. ^{1}H NMR (600 MHz, $CDCl_3$) δ 10.50 (s, 1H), 10.19 (s, 1H), 9.71 (s, 1H), 8.32 (s, 1H), 8.05-7.95 (m, 2H), 7.90 (d, 1H), 7.66 (d, 1H), 7.47 (d, 1H), 7.42-7.35 (m, 4H), 7.32-7.7 (m, 3H), 7.22 (d, 1H), 7.18 (d, 1H), 5.21-5.13 (m, 2H). ^{13}C{^{1}H} NMR (150 MHz, $CDCl_3$) δ 197.0, 192.2, 154.0, 153.6, 138.7, 138.1, 138.0, 136.5, 133.8, 132.7, 130.6, 130.4, 130.0, 129.9, 129.0, 128.54, 128.51, 128.4, 127.7, 127.0, 125.5, 125.1, 124.5, 124.4, 122.2, 119.0, 118.6, 115.8, 70.8. HRMS (ESI-TOF): m/z calcd. for $C_{29}H_{21}O_4$ $[M+H]^+$: 433.1435, found 433.1440. $[\alpha]_D^{24} = -100.2$ (c = 0.2, CH_2Cl_2), mp: 130–132°C.

Synthesis and Characterization of (*R*)-5. (*R*)-**5** was synthesized from the reaction of (*R*)-**7** with 3-bromomethylbenzaldehyde by using the same procedures as the preparation of (*S*)-**4**. Yellow solid, 93.2% yield, 225 mg. ^{1}H NMR (800 MHz, $CDCl_3$) δ 10.50 (s, 1H), 10.19 (s, 1H), 9.71 (s, 1H), 8.32 (s, 1H), 8.05-7.95 (m, 2H), 7.90 (d, 1H), 7.66 (d, 1H), 7.47 (d, 1H), 7.42-7.35 (m, 4H), 7.32-7.7 (m, 3H), 7.22 (d, 1H), 7.19 (d, 1H), 5.21-5.13 (m, 2H). ^{13}C{^{1}H} NMR (200 MHz, $CDCl_3$) δ 197.0, 192.2, 154.0, 153.6, 138.7, 138.1, 138.0, 136.5, 133.8, 132.7, 130.6, 130.4, 130.0, 129.9, 129.0, 128.55, 128.51, 128.4, 127.7, 127.0, 125.5, 125.1, 124.5, 124.4, 122.2, 119.0, 118.6, 115.8, 70.8. HRMS (ESI-TOF): m/z calcd. for $C_{29}H_{21}O_4$ $[M+H]^+$: 433.1435, found 433.1440. $[\alpha]_D^{24} = +99.9$ (c = 0.2, CH_2Cl_2), mp: 129–132°C.

Synthesis and Characterization of (*S*)-6. (*S*)-**6** was synthesized from the reaction of (*S*)-**7** with 4-(bromomethyl) benzaldehyde by using the same procedures as the preparation of (*S*)-**4**. Yellow solid, 98.9%, 597 mg. ^{1}H NMR (600 MHz, $CDCl_3$) δ 10.50 (s, 1H), 10.19 (s, 1H), 9.91 (s, 1H), 8.32 (s, 1H), 8.00 (d, 1H), 7.98 (d, 1H), 7.89 (d, 1H), 7.64 (d, 2H), 7.44-7.34 (m, 4H), 7.29 (t, 1H), 7.2 (d, 1H), 7.19 (d, 1H), 7.14 (d, H), 5.22-5.14 (m, 2H). ^{13}C{^{1}H} NMR (150 MHz, $CDCl_3$) δ 196.9, 192.0, 154.0, 153.6, 144.5, 138.1, 138.0, 135.7, 133.8, 130.5, 130.3, 130.0, 129.8, 128.4, 127.7, 127.1, 127.0, 125.4, 125.1, 124.5, 124.4, 122.2, 118.9, 118.6, 115.7, 70.8. HRMS (ESI-TOF): m/z calcd. for $C_{29}H_{21}O_4$ $[M+H]^+$: 433.1435, found 433.1446. $[\alpha]_D^{24} = -97.1$ (c = 0.2, CH_2Cl_2), mp: 129–131°C.

The Procedure of Sample Preparation for NMR Titration. The following stock solutions were freshly prepared for each measurement: (*S*)-**4**/**5**/**6** (16 mM) in DMSO-d_6, $Zn(OAc)_2$ (64 mM) in DMSO-d_6, and D- or L-LysNa (128 mM) in DMSO-d_6. LysNa was prepared by treating Lys with 1.0 equiv NaOH (in MeOH) followed by removal of the solvent. In each measurement, 150 μL of (*S*)-**4**, 150 μL of 0 ~ 8.0 equiv of D-/L-/rac-LysNa, and 150 μL of DMSO-d_6 were mixed and reacted for 6 h (or as noted). 150 μL of 0.25 ~ 4.0 equiv $Zn(OAc)_2$ or DMSO-d_6 was then added at 2 h reaction time before each measurement. The final concentration of (*S*)-**4**/**5**/**6**: 4.0 mM.

General Procedure for High-Resolution Mass Spectrometry. The samples (in DMSO-d_6) are directly obtained from the NMR titration experiments. In each measurement, a 5.0 μL reaction solution was diluted into 500 μL dry MeOH, and the diluted sample (0.1 μL) was then injected into the instrument directly without pre-separation by chromatography (mobile phase: anhydrous MeOH). Mass spectroscopic analyses were conducted by the University of Illinois at Urbana-Champaign Mass Spectrometry Facility.

General Procedure of Sample Preparation for Fluorescence Measurement. The following stock solutions were freshly prepared for each measurement: (*S*)-**4**/**5**/**6** (1.0 mM) in CH_3CN, an amino acid (20 mM, or as noted) in BICINE buffer (50 mM, pH = 8.4), and $Zn(OAc)_2$ (4.0 mM) in deionized water. In each measurement, 500 μL $Zn(OAc)_2$ (2 equiv) and 500 μL amino acid (10 equiv or other quantity) were mixed. And 1000 μL (*S*)-**4**/**5**/**6** was then added. The resulting solution was allowed to react at

room temperature for 1.5 h, and the fluorescence spectra were then recorded at room temperature.

ASSOCIATED CONTENT

Data Availability Statement

The data underlying this study are available in the published article and its Supporting Information.

Supplementary Information Available

Additional experimental procedures and spectroscopic data are provided.

AUTHOR INFORMATION

Corresponding Author

E-mail: lp6n@virginia.edu (Lin Pu)

ORCID

Lin Pu: 0000-0001-8698-3228

Yifan Mao: 0009-0007-3254-9363

Notes

The authors declare no competing financial interest.

Acknowledgement

We thank the support of the US National Science Foundation (CHE-1855443 and CHE-2153466) for this project. We thank Dr. Jeff Ellena in the department of chemistry at University of Virginia for help on the NMR study.

Keywords: Regioselective; Enantioselective; Chiral macrocycle; Dynamic imine transformation; Fluorescent Probe; Lysine.

References

1. (a) H. Brunner, H. Schiessling. Dialdehyde + Diamine Polymer or Macrocycle? *Angew. Chem., Int. Ed. Engl.*, **1994**, *33*, 125-126. (b) Lin, J.; Zhang, H.-C.; Pu, L. Bisbinaphthyl Macrocycle-Based Highly Enantioselective Fluorescent Sensors for α-Hydroxycarboxylic Acids. *Org. Lett.* **2002**, *4*, 3297–3300. (c) Li, Z.-B.; Lin, J.; Pu, L. A cyclohexyl-1,2-diamine-derived bis(binaphthyl) macrocycle: Enhanced sensitivity and enantioselectivity in the fluorescent recognition of mandelic acid. *Angew. Chem. Int. Ed*. **2005**, *44*, 1690-1693. (d) Li, Z.-B.; Lin, J.; Qin, Y.-C.; Pu, L. Enantioselective fluorescent recognition of a soluble "supported" chiral acid: Toward a new method for chiral catalyst screening. *Org. Lett*. **2005**, *7*, 3441-3444.
2. X. Wu, X. Han, Q. Xu, Y. Liu, C. Yuan, S. Yang, Y. Liu, J. Jiang and Y. Cui. Chiral BINOL-Based Covalent Organic Frameworks for Enantioselective Sensing. *J. Am. Chem. Soc*. **2019**, 141, 7081–7089.
3. C. Liu, Y. Jin, D. Qi, X. Ding, H. Ren, H. Wang, J. Jiang. Enantioselective assembly and recognition of heterochiral porous organic cages deduced from binary chiral components. *Chem. Sci*. **2022**, *13*, 7014–7020.
4. (a) J.-M. Lehn. Dynamic Combinatorial Chemistry and Virtual Combinatorial Libraries. *Chem. Eur. J.*, **1999**, *5*, 2455-2463. (b) P. T. Corbett, J. Leclaire, L. Vial, K. R. West, J.-L. Wietor, J. K. M. Sanders, S. Otto. Dynamic Combinatorial Chemistry. *Chem. Rev.*, **2006**, *106*, 3652-3711. (c) C. D. Meyer, C. S. Joiner, J. F. Stoddart. Template-directed synthesis employing reversible imine bond formation. *Chem. Soc. Rev.*, **2007**, *36*, 1705.
5. (a) M. Belowich, J. F. Stoddart. Dynamic imine chemistry. *Chem. Soc. Rev.*, **2012**, *41*, 2003-2024. (b) G. Zhang, M. Mastalerz. Organic cage compounds – from shape-persistency to function. *Chem. Soc. Rev.*, **2014**, *43*, 1934-1947. (c) J. L. Segura, M. J. Mancheño, F. Zamora. Covalent organic frameworks based on Schiff-base chemistry: synthesis, properties, and potential applications. *Chem. Soc. Rev.*, **2016**, *45*, 5635-5671. (d) D. Zhang, T. K. Ronson, J. R. Nitschke. Functional Capsules via Subcomponent Self-Assembly. *Acc. Chem. Res.*, **2018**, *51*, 2423-2436.
6. (a) A. Star, I. Goldberg, B. Fuchs. Dioxadiazadecalin/Salen Tautomeric Macrocycles and Complexes: Prototypal Dynamic Combinatorial Virtual Libraries. *Angew. Chem. Int. Ed.*, **2000**, *39*, 2685-2689. (b) J. Gawronski, H. Kolbon, M. Kwit, A. Katrusiak. Designing Large Triangular Chiral Macrocycles: Efficient [3 + 3] Diamine−Dialdehyde Condensations Based on Conformational Bias. *J. Org. Chem.*, **2000**, *65*, 5768-5773. (c) N. Kuhnert, A. M. Lopez-Periago. Synthesis of novel chiral non-racemic substituted trianglimine and trianglamine macrocycles. *Tetrahedron Lett.*, **2002**, *43*, 3329-3332. (d) M. Kwit, J. Gawrosky. Chiral calixsalen-type macrocycles from trans-1,2-diaminocyclohexane. *Tetrahedron: Asymmetry*, **2003**, *14*, 1303-1308. (e) N. Kuhnert, G. M. Rossignolo, A. López-Periago. The synthesis of trianglimines: on the scope and limitations of the [3 + 3] cyclocondensation reaction between (1R,2R)-diaminocyclohexane and aromatic dicarboxaldehydes. *Org. Biomol. Chem.*, **2003**, *1*, 1157-1170. (f) A. González-Álvarez, I. Alfonso, F. López-Ortiz, Á. Aguirre, S. García-Granda, V. Gotor. Selective Host Amplification from a Dynamic Combinatorial Library of Oligoimines for the Syntheses of Different Optically Active Polyazamacrocycles. *Eur. J. Org. Chem.*, **2004**, 1117.
7. (a) D. Beaudoin, F. Rominger, M. Mastalerz. Chiral Self-Sorting of [2 + 3] Salicylimine Cage Compounds. *Angew. Chem., Int. Ed.*, **2017**, *56*, 1244-1248. (b) D. Xu, R. Warmuth. Edge-Directed Dynamic Covalent Synthesis of a Chiral Nanocube. *J. Am. Chem. Soc.*, **2008**, *130*, 7520-7521. (c) T. Hasell, S. Y. Chong, K. E. Jelfs, D. J. Adams, A. I. Cooper. Porous Organic Cage Nanocrystals by Solution Mixing. *J. Am. Chem. Soc.*, **2012**, *134*, 588-598. (d) E. Jelfs Kim, X. Wu, M. Schmidtmann, J. T. A. Jones, J. E. Warren, D. J. Adams, A. I. Cooper. Large Self-Assembled Chiral Organic Cages: Synthesis, Structure, and Shape Persistence. *Angew. Chem.*, **2011**, *123*, 10841-10844.
8. A communication of this work was reported: Mao, Y.; Davis, S.; Pu, L. Regio- and Enantioselective Macrocyclization from Dynamic Imine Formation: Chemo- and Enantioselective Fluorescent Recognition of Lysine. *Org. Lett*. **2023**, *25*, 7639-7644.
9. P. Kovaricek, J.-M. Lehn. Merging Constitutional and Motional Covalent Dynamics in Reversible Imine Formation and Exchange Processes. *J. Am. Chem. Soc.*, **2012**, *134*, 9446-9455.
10. (a) Zhu, Y.; Wu, X.; Gu, S.; Pu, L. Free Amino Acid Recognition: A bisbinaphthyl-based fluorescent probe with high enantioselectivity. *J. Am. Chem. Soc*. **2019**, *141*, 175–181. (b) Y. Mao, M. Abed, N. B. Lee , X. Wu, G. Du and L. Pu. Determine Concentration and Enantiomeric Composition of Histidine by One Fluorescent Probe. *Chem. Commun*. **2021**, 57, 587-590.
11. (a) Huang, Z.; Yu, S. S.; Yu, X. Q.; Pu. L. Zn(II) Promoted Dramatic Enhancement in the Enantioselective Fluorescent Recognition of Chiral Amines by a Chiral Aldehyde. *Chem. Sci.* **2014**, *5*, 3457-3462. (b) Mao, Y.; Thomae, E.; Davis, S.; Wang, C.; Li, Y.; Pu, L. One Molecular Probe with Opposite Enantioselective Fluorescence Enhancement at Two Distinct Emissions. *Org. Lett*. **2023**, *25*, 2157-2161.
12. (a) Wu, G. Amino acids: metabolism, functions, and nutrition. *Amino Acids* **2009**, *37*, 1–17. (b) Tomé, D.; Bos, C. Lysine requirement through the human life cycle. *J. Nutrition* 2007*, 137,* 1642S–1645S.
13. (a) Miyamoto, T.; Homma, H. D-Amino acid metabolism in bacteria. *J. Biochem*. **2021**, *170*, 5–13. (b) Zabriskie, T. M.; Jackson, M. D. Lysine biosynthesis and metabolism in fungi. *Nat. Prod. Rep*. **2000**, *17*, 85–97.
14. Verma, D. P.; Ansari, M. M.; Verma, N. K.; Saroj, J.; Akhtar, S.; Pant, G.; Mitra, K.; Singh, B. N.; Ghosh, J. K. Tandem Repeat of a Short Human Chemerin-Derived Peptide and Its Nontoxic D-Lysine-Containing Enantiomer Display Broad-Spectrum

Antimicrobial and Antitubercular Activities. *J. Med. Chem.* **2021**, 64, 20, 15349–15366

15. (a) Pu, L. Enantioselective Fluorescent Recognition of Free Amino Acids: Challenges and Opportunities. *Angew. Chem. Int. Ed*. **2020**, *59*, 21814-21828. (b) Zhou, Y.; Yoon, J. Recent Progress in Fluorescent and Colorimetric Chemosensors for Detection of Amino Acids. *Chem. Soc. Rev*. **2012**, *41*, 52–67. (c) Wang, J.; Liu, H.-B.; Tong, Z.; Ha, C.-S. Fluorescent/Luminescent Detection of Natural Amino Acids by Organometallic Systems. *Coord. Chem. Rev*. **2015**, *303*, 139-184.
16. (a) Yang, B.; Zhou, J.; Huang, X.; Chen, Z.; Tian, S.; Shi, Y. A New Pyrroloquinoline-Derivative-Based Fluorescent Probe for the Selective Detection and Cell Imaging of Lysine. *Pharmaceuticals* **2022**, *15*, 474. (b) Ma, H.; Qi, C.; Cao, H.; Zhang, Z.; Yang, Z.; Zhang, B.; Chen, C.; Lei, Z.Q. Water-soluble fluorescent probes for selective recognition of lysine and its application in an object carry-and-release system. *Chem. Asian J.* **2016**, *11*, 58–63. (c) Zhou, Y.; Won, J.; Lee, J.Y.; Yoon, J. Studies leading to the development of a highly selective colorimetric and fluorescent chemosensor for lysine. *Chem. Commun.* **2011**, *47*, 1997–1999. (d) Lohar, S.; Safin, D. A.; Sengupta, A.; Chattopadhyay, A.; Matalobos, J.S.; Babashkina, M.G.; Robeyns, K.; Mitoraj, M.P.; Kubisiak, P.; Garcia, Y.; Das, D. Ratiometric sensing of lysine through the formation of the pyrene excimer: Experimental and computational studies. *Chem. Commun*. **2015**, *51*, 8536–8539. (e) Adhikari, S.; Ghosh, A.; Mandal, S.; Guria, S.; Banerjee, P.P.; Chatterjee, A.; Das, D. Colorimetric and fluorescence probe for the detection of nano-molar lysine in aqueous medium. *Org. Biomol. Chem*. **2016**, *14*, 10688–10694. (f) Yang, L.; Xie, Y.; Chen, Q.; Zhang, J.; Li, L.; Sun, H. Colorimetric and fluorescent dual-signal chemosensor for lysine and arginine and its application to detect amines in solid-phase peptide synthesis. *ACS Appl. Bio Mater*. **2021**, *4*, 6558–6564. (g) Zhu, Z.; Wang, Y.; Ding, H.; Fan, C.; Tu, Y.; Liu, G.; Pu, S. A novel full symmetric diarylethene-based ratiometric fluorescent sensor for lysine and the application for a logic circuit. *Luminescence* **2021**, *36*, 691–697. (h) Hou, J.-T.; Li, K.; Liu, B.-Y.; Liao, Y.-X.; Yu, X.-Q. The first ratiometric probe for lysine in water. *Tetrahedron* **2013**, *69*, 2118–2123. (i) Qian, X.; Gong, W.; Wang, F.; Lin, Y.; Ning, G. A pyrylium-based colorimetric and fluorimetric chemosensor for the selective detection of lysine in aqueous environment and real sample. *Tetrahedron Lett*. **2015**, *56*, 2764–2767. (j) K. Secor, J. Plante, C. Avetta, T. Glass. Fluorescent sensors for diamines. *J. Mater. Chem*. **2005**, *15*, 4073–4077.
17. (a) Du, G.; Pu, L. Micelle-encapsulated fluorescent probe: Chemoselective and enantioselective recognition of lysine in aqueous solution. *Org. Lett*. **2019**, *21*, 4777–4781. (b) Yang, J.; Jiang, L.; Tian, J.; Yu, S.; Yu, X.; Pu, L. Fluorous Phase-Enhanced Fluorescent Sensitivity for Enantioselective Recognition of Lysine. *Org. Lett.* **2022**, *24*, 9327–9331.